AD-A031 626 HARVARD UNIV CAMBRIDGE MASS DIV OF ENGINEERING AND --ETC F/G 11/6
A MICROSCOPIC MECHANISM FOR STEADY STATE INHOMOGENEOUS FLOW IN --ETC(U)
AUG 76 F SPAEPEN N00014-67-A-0298-0036
UNCLASSIFIED TR-7 NL

| OF |
AD
A031 626

END

DATE
FILMED
12-76

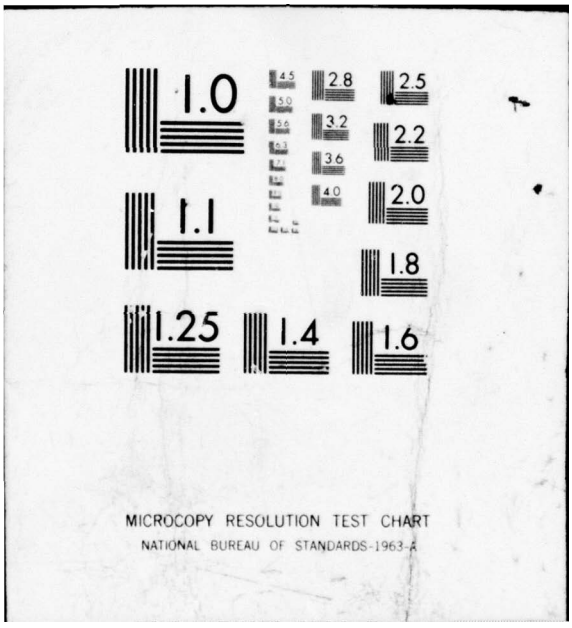
1.0
1.1
1.25
1.4
1.6
1.8
2.0
2.2
2.5
2.8
3.2
3.6
4.0
4.5
5.0
5.6
MICROCOPY RESOLUTION TEST CHART
NATIONAL BUREAU OF STANDARDS-1963-A

Office of Naval Research
Contract N00014- 67-A-0298-0038 NR-032-544
National Science Foundation Grant DMR-72-03020

A MICROSCOPIC MECHANISM FOR STEADY STATE INHOMOGENEOUS FLOW IN METALLIC GLASSES

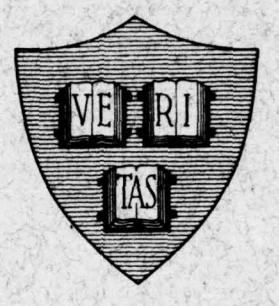

By

Frans Spaepen

August 1976

Technical Report No. 7

Division of Engineering and Applied Physics
Harvard University • Cambridge, Massachusetts

Unclassified

SECURITY CLASSIFICATION OF THIS PAGE *(When Data Entered)*

REPORT DOCUMENTATION PAGE

READ INSTRUCTIONS BEFORE COMPLETING FORM

1. REPORT NUMBER: Technical Report No. 7 ✓
2. GOVT ACCESSION NO.
3. RECIPIENT'S CATALOG NUMBER: (9) technical

4. TITLE *(and Subtitle)*: (6) A MICROSCOPIC MECHANISM FOR STEADY STATE INHOMOGENEOUS FLOW IN METALLIC GLASSES.

5. TYPE OF REPORT & PERIOD COVERED: Interim Report.

6. PERFORMING ORG. REPORT NUMBER

7. AUTHOR(s): (10) Frans Spaepen

8. CONTRACT OR GRANT NUMBER(s): (15) N00014-67-A-0298-0036, NSF-Grant DMR-72-03020

9. PERFORMING ORGANIZATION NAME AND ADDRESS: Division of Engineering and Applied Physics ✓, Harvard University, Cambridge, Massachusetts 02138

10. PROGRAM ELEMENT, PROJECT, TASK AREA & WORK UNIT NUMBERS: 032-544

11. CONTROLLING OFFICE NAME AND ADDRESS: (12) 34p.

12. REPORT DATE: (11) August 1976

13. NUMBER OF PAGES: 34

14. MONITORING AGENCY NAME & ADDRESS *(if different from Controlling Office)*: (14) TR-7

15. SECURITY CLASS. *(of this report)*: Unclassified

15a. DECLASSIFICATION/DOWNGRADING SCHEDULE

16. DISTRIBUTION STATEMENT *(of this Report)*

This document has been approved for public release and sale; its distribution is unlimited. Reproduction in whole or in part is permitted by the U.S. Government.

17. DISTRIBUTION STATEMENT *(of the abstract entered in Block 20, if different from Report)*

18. SUPPLEMENTARY NOTES

19. KEY WORDS *(Continue on reverse side if necessary and identify by block number)*

Empirical deformation map
Metallic glasses

20. ABSTRACT *(Continue on reverse side if necessary and identify by block number)*

An empirical deformation map for metallic glasses is introduced and the two modes of deformation, homogeneous and inhomogeneous flow are reviewed. The microscopic mechanism for steady state inhomogeneous flow is based on a dynamic equilibrium between stress-driven creation and diffusional annihilation of structural disorder. The formalism is developed using the free volume as the order parameter. The boundary line between the homogeneous and inhomogeneous flow regions on the deformation map is calculated. The stress-strain relation in inhomogeneous flow approaches ideally

→over

DD FORM 1 JAN 73 1473 EDITION OF 1 NOV 65 IS OBSOLETE S/N 0102-014-6601 |

Unclassified 163 750

SECURITY CLASSIFICATION OF THIS PAGE *(When Data Entered)*

4B

plastic behavior.

Office of Naval Research

Contract N00014-67-A-0298-0036 NR-032-544

National Science Foundation Grant DMR-72-03020

A MICROSCOPIC MECHANISM FOR STEADY STATE INHOMOGENEOUS FLOW IN METALLIC GLASSES

By

Frans Spaepen

Technical Report No. 7

August 1976

The research reported in this document was made possible through support extended the Division of Engineering and Applied Physics, Harvard University by the U. S. Army Research Office, the U. S. Air Force Office of Scientific Research and the U. S. Office of Naval Research under the Joint Services Electronics Program by Contract N00014-67-A-0298-0036 and by the National Science Foundation under Grant DMR-72-03020.

Division of Engineering and Applied Physics

Harvard University · Cambridge, Massachusetts

ABSTRACT

An empirical deformation map for metallic glasses is introduced and the two modes of deformation, homogeneous and inhomogeneous flow are reviewed. The microscopic mechanism for steady state inhomogeneous flow is based on a dynamic equilibrium between stress-driven creation and diffusional annihilation of structural disorder. The formalism is developed using the free volume as the order parameter. The boundary line between the homogeneous and inhomogeneous flow regions on the deformation map is calculated. The stress-strain relation in inhomogeneous flow approaches ideally plastic behavior.

1. INTRODUCTION: AN EMPIRICAL DEFORMATION MAP FOR METALLIC GLASSES

The deformation map, developed by Ashby and Frost for crystalline systems[1-3] is a convenient means of surveying the various modes of plastic deformation of a material. To construct a map, each mode of deformation is described by a steady state constitutive flow law:

$$\dot{\gamma} = f(\tau, T, \text{structure})$$

where $\dot{\gamma}$ is the shear strain rate, τ the shear stress, T the temperature; "structure" represents all the relevant structural parameters of the material. The steady state condition implies that the structural parameters are uniquely determined by the external parameters stress and temperature, and hence remain constant during the course of the flow. An appropriate superposition of the flow mechanisms makes it possible to draw constant $\dot{\gamma}$ contours on a map with axes τ and T (usually normalized by the shear modulus μ and the melting point T_M, respectively), and to outline regions in which each of the various mechanisms is dominant.

Plotting experimental flow data $\dot{\gamma}(\tau, T)$ in the same coordinate system results in an empirical deformation map. A comparison of the calculated and empirical maps provides a test of the flow equations. But even if no calculated map is available yet, an empirical map is useful for surveying the data and outlining the various flow mechanisms. Therefore, the available flow data for Pd-based metallic glasses are presented on such an empirical map in Fig. 1. Ideally, only data obtained from samples with identical composition should be compared,

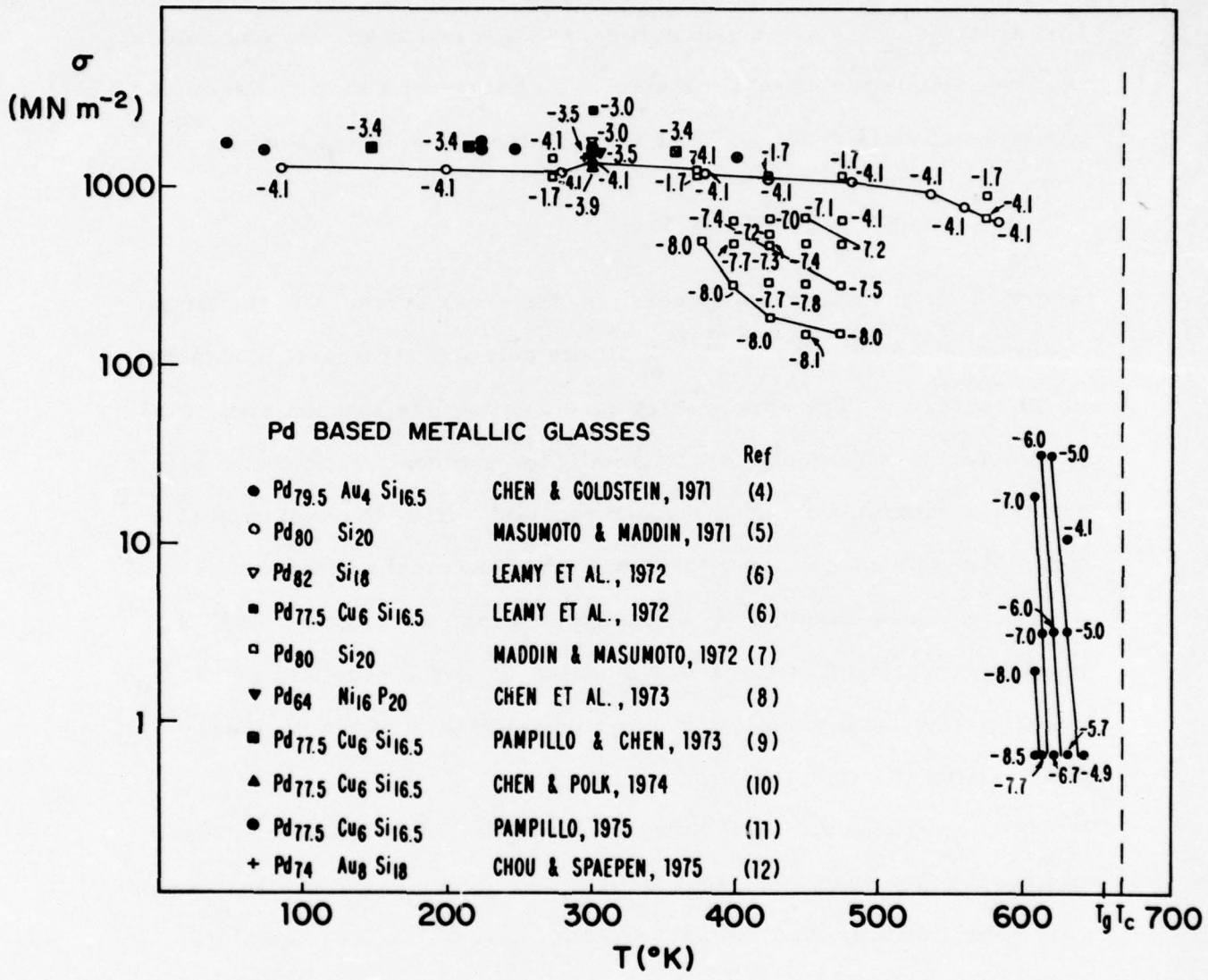

Empirical deformation map for Pd-based metallic glasses. The number at each data point is $\log \dot{\epsilon}$ (in $\sec^{-1}$). Both stress (σ) and strain rate ($\dot{\epsilon}$) are uniaxial. The glass transition temperature (T_g) and the crystallization temperature (T_c) are for $Pd_{80}Si_{20}$ (Ref. 13).

Figure 1

but the relative paucity of the data, together with the large flexibility in preparing amorphous metal alloy compositions make it necessary to group the data together according to their major constituent. With one exception, all the alloys represented in Fig. 1 contain 74-82 at % Pd and 16.5-20 at % Si. Their structural characteristics (density, radial distribution function, modulus, ...) and transformation parameters (glass transition temperature T_g, crystallization temperature T_c, heat of crystallization) vary within acceptable limits, given the typical accuracy of mechanical testing. Since all the data were obtained in either uniaxial tension or compression, the stress (σ) and strain rate ($\dot{\epsilon}$) are plotted as such and have not been converted to the equivalent shear quantities. Where possible, some approximate constant strain rate contours have been drawn in. The flow stresses obtained from creep tests,[4,7] compression tests,[9,10,11] and ultimate tensile strength measurements (the three highest temperature points in Masumoto and Maddin's tensile tests[5]) are probably close to the steady state values. In the other tensile tests,[5-8,12] however, fracture intervenes before steady state is reached. In these cases, the fracture stress has been plotted, since it comes closest to the steady state value. Above T_ℓ (the liquidus temperature of the crystalline material with the same composition--not shown in Fig. 1) flow is measured by viscometric methods. No measurements of this type have been reported for Pd-based glasses, but experience from other liquid metal alloys[14] shows that the viscosity in this temperature regime is usually around 10^{-3} $Nm^{-2}sec$.

Based on this empirical information, it is now possible to show an approximate picture of what a calculated map should look like. Such

a schematic map, with stress and temperature axes extended further than in Fig. 1, is shown in Fig. 2. The temperature region between T_c and T_ℓ is unaccessible for mechanical measurements because crystallization intervenes, but it is possible to make a reasonable extrapolation of the strain rate contours through this region.

2. THE FLOW MECHANISMS

Inspection of the samples and fracture surfaces after testing shows that there are two basic modes of deformation: homogeneous flow, where each volume element of the specimen contributes to the strain, and inhomogeneous flow, where the strain is localized in a few very thin shear bands.

a. Homogeneous Flow

As indicated on Fig. 2, this mode of deformation occurs at low stresses and high temperatures. In this regime, the flow is close to Newtonian viscous (i.e., $\dot{\gamma} \propto \tau$), as is clear from the spacing of the strain rate contours on the map. In uniaxial tension, a specimen thins down uniformly during deformation. Fracture occurs after extensive plastic flow, when some section of the specimen has narrowed down to zero thickness. For convenience, the region of homogeneous deformation can be subdivided, admittedly somewhat arbitrarily, in three parts, depending on the viscosity of the material.

(i) for $T > T_\ell$, the material has a viscosity $\eta \approx 10^{-3} Nm^{-2} sec.$, and can be characterized as "fluid". Flow measurements must

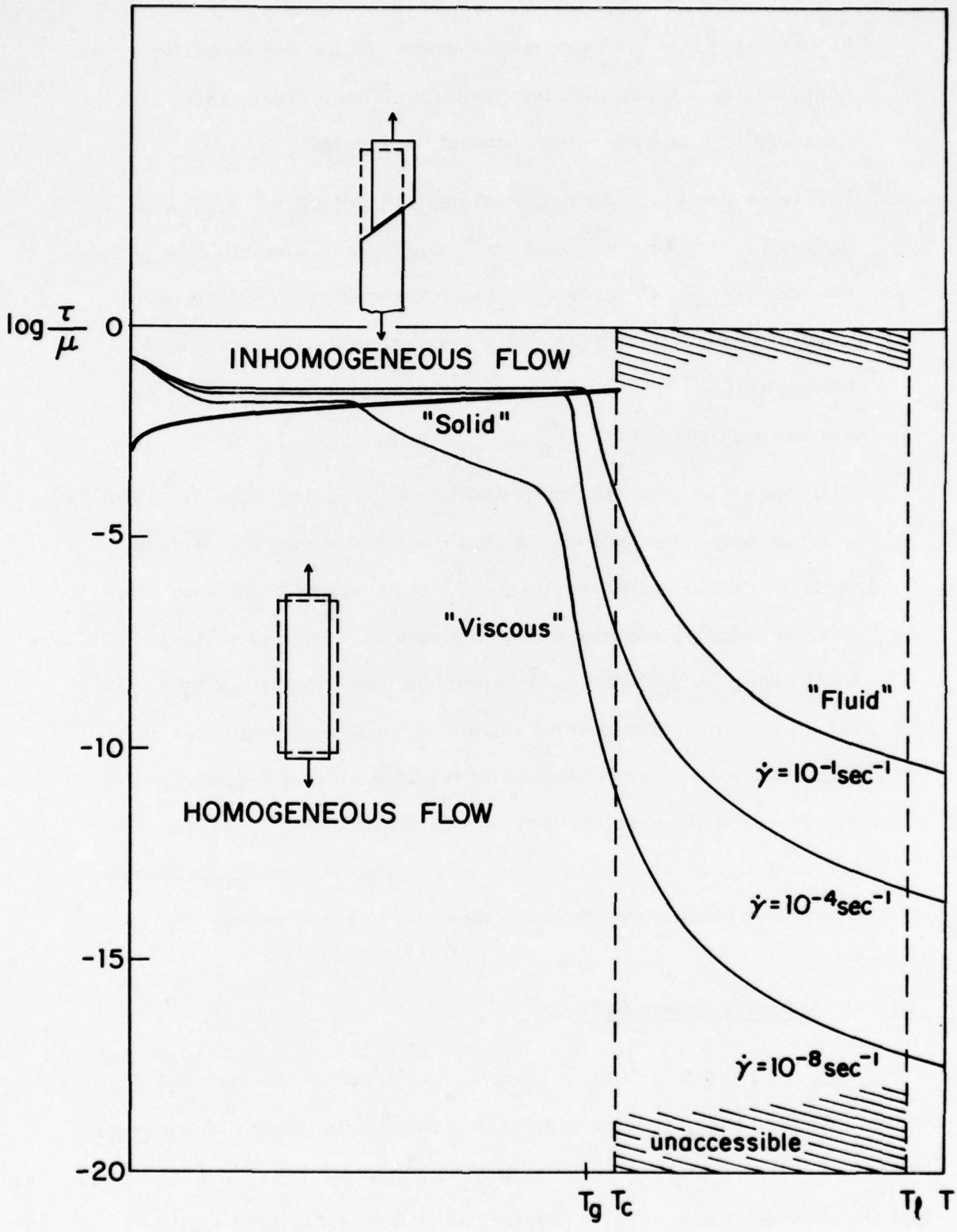

Schematic deformation map of a metallic glass. The various modes of deformation are indicated.

Figure 2.

be performed by viscometric methods. Since the viscosity changes only slowly with temperature,[14] the strain rate contours in this regime are almost horizontal.

(ii) for $T \approx T_g$, the material has, by definition of T_g, a viscosity between 10^{15} and 10^{10} $Nm^{-2}sec.$, and could be called "viscous". In this regime, the viscosity, which is measured in a creep test, falls very steeply with increasing temperature.[4, 15] Consequently, the strain rate contours are almost vertical around T_g.

(iii) for $T < T_g$, the material has a viscosity $\eta > 10^{15}$ $Nm^{-2}sec.$, and can be called "solid". From the limited number of creep tests available in this regime,[7, 16] it seems that the viscosity does not change rapidly with temperature, which is reflected on the map by the strain rate contours becoming more horizontal. However, conclusions about flow in this region must be regarded with caution because of the limited number of experiments available, and the largely unstudied influence of the thermal and mechanical history of the material on the properties. Some careful investigations of these effects are necessary.

b. Inhomogeneous Flow

This mode of deformation occurs at high stress levels (see Fig. 2). In this regime, the stress is very strain rate insensitive (or, in other words: the stress exponent $n = \partial \log \dot{\gamma} / \partial \log \tau$ is very large), so that the flow is almost ideally plastic. The flow stress for a given strain rate, when normalized by the temperature dependent shear

modulus (i.e., τ/μ), is almost constant with temperature, except at low temperatures and near T_g. On the deformation map, this results in very closely spaced, almost horizontal strain rate contours.

In inhomogeneous flow the strain is localized in a few very thin shear bands. In ribbons pulled in tension these shear bands are planes, usually perpendicular to the thin side of the ribbon and at a 45^o angle with the tensile axis.[5,6,17] Slip on these planes can be very extensive. This weakens the specimen locally by decreasing the cross section, until finally fracture occurs along the planes of those shear bands.[6,12] The fracture surface exhibits a typical vein-like pattern,[6,12,18] which indicates that the mechanism of fracture is the Taylor instability.[18-20]

The basic physical process underlying this inhomogeneous flow phenomenon is a local softening of the material. This becomes clear from a number of observations.

(i) localization of the flow in shear bands requires that there is some structural change of the material inside the bands, such that they deform much faster there than in the rest of the specimen.[20]

(ii) fracture in a tensile specimen occurs, as indicated above, along the plane of a shear band, which makes a 45^o angle with the tensile axis. Ordinarily, one would expect fracture to occur along the plane of maximum normal stress, i.e., normal to the tensile axis. This means that if fracture occurs along a shear plane with a smaller resolved normal stress, the material along this plane must have been weakened by some shear-related structural change.

(iii) the vein pattern on the fracture surface is very similar to that obtained by the pulling apart of two solid surfaces containing a thin viscous layer between them.[8,21,22] This observation is consistent with (ii): the shear band consists of a layer of material with a viscosity lower than that of the rest of the specimen, which weakens the plane against fracture by the Taylor instability mechanism.

(iv) differential etching of the shear bands after deformation[23,24] indicates that there are chemical changes associated with flow. This is to be expected if the shear-induced structural changes do not completely relax out after removal of the load.

3. THE GENERAL FLOW EQUATION

The microscopic mechanism which governs both homogeneous and inhomogeneous flow is illustrated by Fig. 3. It is assumed that macroscopic flow occurs as a result of a number of individual atomic jumps. In order for an atom to jump, it must have a nearest neighbor environment as shown in Fig. 3, i.e., next to it there must be a hole large enough to accomodate its (appropriate hard-sphere equivalent) atomic volume v^*. It is reasonable to assume that the atomic positions before and after the jump are positions of relative stability, i.e., local free energy minima. In order to make the atom jump, some activation energy of motion ΔG^m must be supplied. If no external force is present, this is obtained from thermal fluctuations; the number of jumps across the activation barrier is the same in both directions; this is the basic microscopic mechanism for diffusion. When an

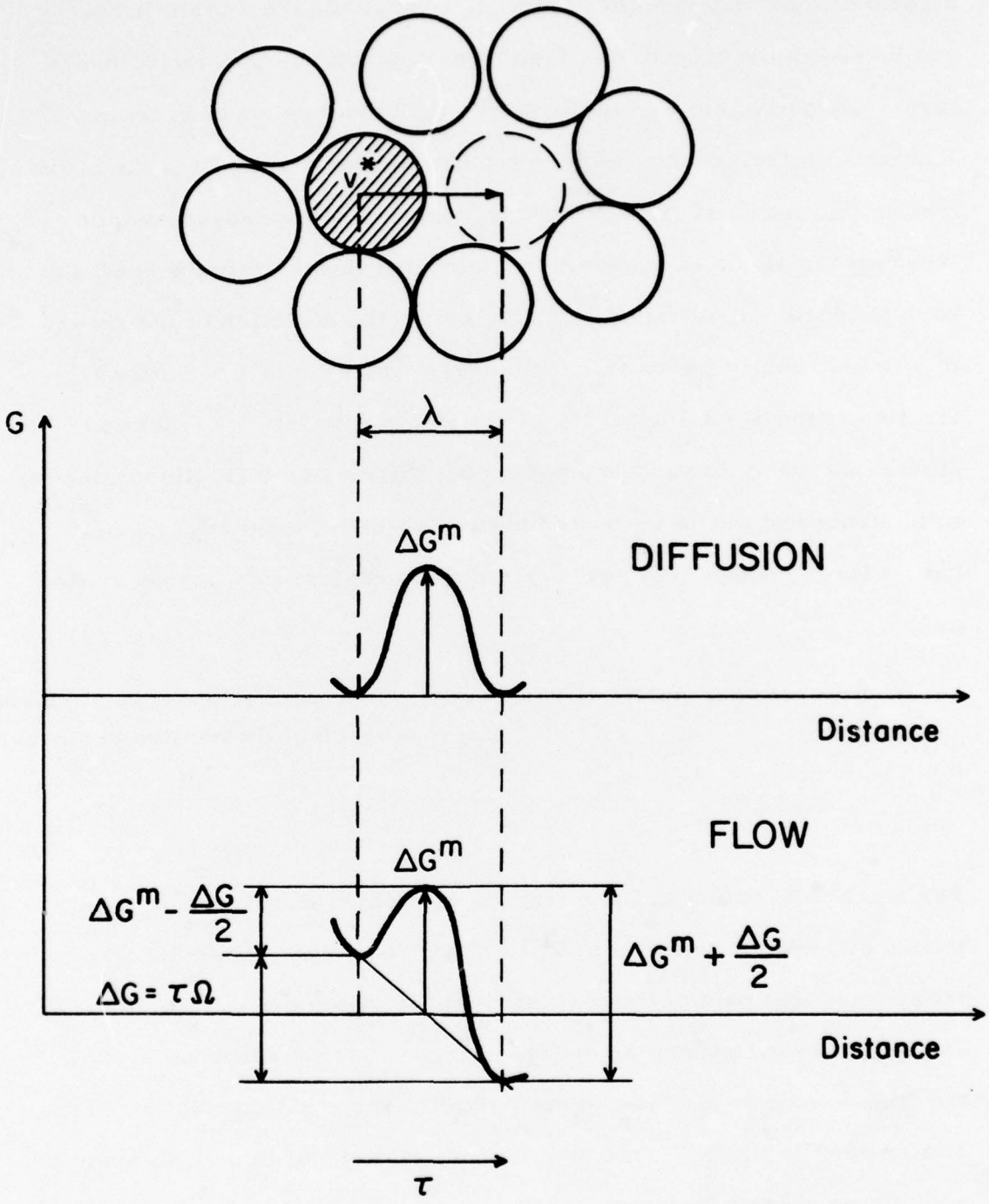

Illustration of an individual atomic jump, the basic step for macroscopic diffusion and flow.

Figure 3.

external force, e.g., a shear stress, is applied, the atomic jumps are biased in the direction of the force; the number of forward jumps across the activation barrier is larger than the number of backward jumps; this results in a net forward flux of atoms and forms the basic mechanism for flow. Quantitatively, this can be expressed as follows. When <u>all</u> the atoms in a specimen, deformed in shear, make one jump each of length λ ($\approx$ 1 atomic diameter) in the direction of the shear, this would result in a macroscopic shear strain $\gamma \approx 1$. If only a fraction of the atoms jump, the shear strain rate is: $\dot{\gamma}$ = fraction of atoms that make forward jumps/second. Since only a fraction of the total number of atoms in the sample are potential jump sites, i.e., have a large enough hole next to them as in Fig. 3, this can be written as

$$\dot{\gamma} = \text{(fraction of potential jump sites)} \times \text{(net number of forward jumps on each of those sites per second)} \qquad (1)$$

The fraction of potential jump sites is calculated in the free volume theory of Turnbull and Cohen.[25-27] The free volume of an atom is, intuitively, that part of its nearest neighbor cage in which the atom can move around without an energy change. In an amorphous system, the free volume is distributed statistically among all atoms. In Cohen and Turnbull's theory[25] the probability $p(v)\,dv$ of finding an atom with a free volume between v and $v + dv$ is calculated to be:

$$p(v)\,dv = \frac{\gamma}{v_f} \exp\left(-\frac{\gamma v}{v_f}\right) dv$$

where γ is a geometrical factor between 1 and 1/2, and v_f is the average free volume of an atom.

In order for an atom to be on a potential jump site, its free volume must be larger than v^*, the effective hard-sphere size of the atom. Therefore, the total probability that an atom is on a potential jump site is:

$$\int_{v^*}^{\infty} \frac{\gamma}{v_f} \exp\left(-\frac{\gamma v}{v_f}\right) dv = \exp\left(-\frac{\gamma v^*}{v_f}\right) \qquad (2)$$

It is also necessary to include a factor Δf, the fraction of the sample volume in which potential jump sites can be found. For example, in homogeneous flow, where the total volume contributes to flow, $\Delta f = 1$; in inhomogeneous flow, where everything happens in a few very thin bands, $\Delta f \ll 1$. Therefore,

$$\text{fraction of potential jump sites} = \Delta f \exp(-\gamma v^*/v_f) \qquad (3)$$

The net number of forward jumps per second on a potential jump site is obtained from simple rate theory (see Fig. 3). The shear stress τ exerts a force τa on an atom, where a is the projected area of the atom onto the plane of shear. When this atom makes a jump of length λ, the work done is $\tau a \lambda$. Since λ is roughly equal to an atomic diameter, the work done is $\tau\Omega$ where Ω is the atomic volume. The free energy of the atom after the jump is therefore decreased by $\Delta G = \tau\Omega$. The net number of forward jumps per second can now be calculated as the difference between a forward flux over an activation barrier $\Delta G^m - \Delta G/2$ and a backward flux over an activation barrier $\Delta G^m + \Delta G/2$. Assuming an equal distribution of atoms over the two

equilibrium positions gives:

net number of forward jumps per second per potential jump site

$$= \upsilon \exp\left(-\frac{\Delta G^m - \tau\Omega/2}{kT}\right) - \exp\left(-\frac{\Delta G^m + \tau\Omega/2}{kT}\right) \qquad (4)$$

where υ is the frequency of atomic vibration ($\sim$ Debye frequency). Substituting (3) and (4) into (1) gives:

$$\dot{\gamma} = \Delta f \exp\left(-\frac{\gamma v^*}{v_f}\right) 2\upsilon \sinh\left(\frac{\tau\Omega}{2kT}\right) \exp\left(-\frac{\Delta G^m}{kT}\right) \qquad (5)$$

This is the general flow equation. In the case of homogeneous deformation ($\Delta f = 1$) at low stress levels ($\tau\Omega \ll 2kT$), this leads to Newtonian viscous behavior ($2 \sinh(\tau\Omega/2kT) \approx \tau\Omega/kT$), and an expression for the viscosity can be derived:

$$\eta = \frac{\tau}{\dot{\gamma}} \approx \frac{kT}{\upsilon\Omega} \exp\left(\frac{\gamma v^*}{v_f}\right) \exp\left(\frac{\Delta G^m}{kT}\right) \qquad (6)$$

The diffusion coefficient in a three dimensional random walk process is defined as $D = \frac{1}{6}\Gamma\lambda^2$ where Γ and λ are the jump frequency and distance, respectively. An analysis, similar to that of the flow problem gives:

Γ = (probability that an atom is on a potential jump site)
× (number of jumps an atom on this site makes per second)

or:

$$\Gamma = \exp\left(-\frac{\gamma v^*}{v_f}\right) \upsilon \exp\left(-\frac{\Delta G^m}{kT}\right) \qquad (7)$$

This gives for the diffusion coefficient:

$$D = \frac{1}{6}\upsilon \exp\left(-\frac{\gamma v^*}{v_f}\right)\exp\left(-\frac{\Delta G^m}{kT}\right)\lambda^2 \qquad (8)$$

It is worth noting that combining Equations (6) and (8) gives

$$D\eta = \frac{kT}{6(\Omega/\lambda^2)}$$

which is, save for a numerical factor of order 1, the Stokes-Einstein equation.

4. THE SOFTENING MECHANISM IN INHOMOGENEOUS FLOW

As has been discussed in Section 2b, during inhomogeneous flow, the material in the shear bands undergoes some structural change that leads to a local lowering of the viscosity.

Polk and Turnbull[14] have proposed that this structural change is the net result of two competing processes: a shear-induced disordering and a diffusion controlled reordering process. This concept will be extended here, by deriving a formal expression for the dynamic steady state equilibrium between the two processes. The free volume will be chosen as the order parameter, since it makes the problem mathematically tractable. It should be kept in mind, however, that to the extent that the free volume is equivalent to other possible order parameters (compositional, entropic,...), the result should be quite generally valid.

In the free volume formulation of the flow Equation (5), the structural parameter which governs the viscosity is the average free volume v_f. Therefore, if there is to be a lowering of the viscosity in the shear bands, there must be an increase of the free volume.

It is proposed that, at high stress levels, free volume can be created by the mechanism shown on Fig. 4. At a sufficiently high stress, an atom with hard-sphere volume v^* can be squeezed into a neighboring hole with a smaller volume v. This makes the neighbors of the new position move out, and creates a certain amount of free volume.

Competing with this is a relaxation process, which tends to annihilate the extra free volume created and restore the system to its initial structural state. The structural rearrangements necessary to annihilate free volume consist of a series of diffusional jumps.

In steady state a dynamic equilibrium is reached between the two competing processes: an equal amount of free volume is created by the stress-driven process, as is annihilated by the diffusional process.

a. Creation of Free Volume

The energy necessary to squeeze an atom with volume v^* into a smaller hole of volume v (see Fig. 4) can be approximated by the elastic distortion energy required to squeeze a sphere with volume v^* into a spherical hole with volume v in a matrix of the same material. This has been calculated by Eshelby:[28]

$$\Delta G^e = S \frac{(v^* - v)^2}{v}$$

with

$$S = \frac{2}{3} \mu \frac{1+\upsilon}{1-\upsilon}$$

If an atom makes the jump over the activation barrier in the direction of shear, its free energy is decreased by the driving term $\tau\Omega$ (see

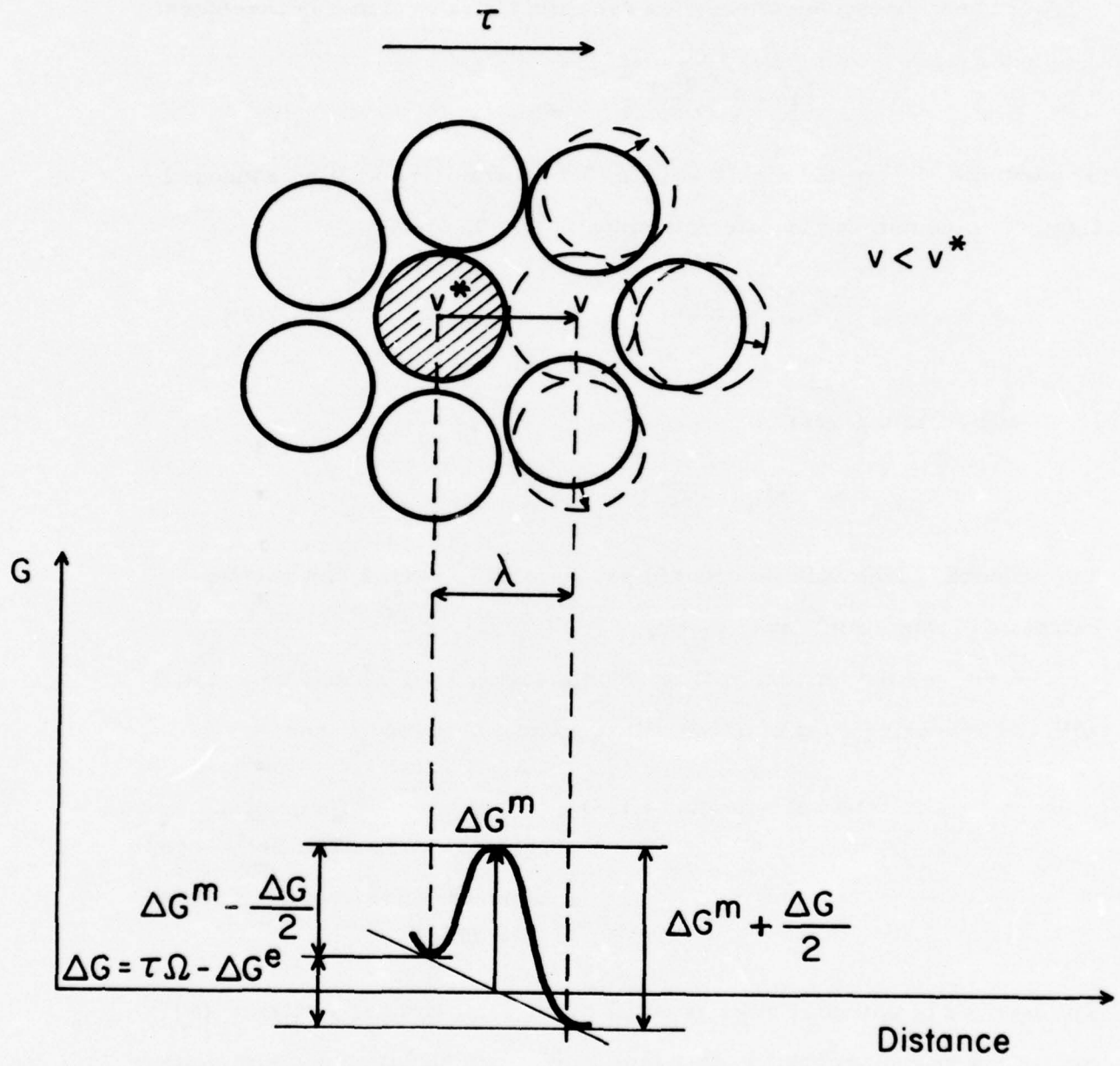

Illustration of the creation of free volume, by squeezing an atom of volume v* into a neighboring hole of smaller volume v.

Figure 4.

Section 3), but it is also increased by the elastic distortion energy ΔG^e. The driving free energy for creation of free volume is therefore:

$$\Delta G = \tau\Omega - S\frac{(v^* - v)^2}{v}$$

The volume v_m of the smallest hole that an atom can still be squeezed into by a given stress is determined by $\Delta G = 0$, or:

$$\tau\Omega = S\frac{(v^* - v_m)^2}{v_m} \qquad (7)$$

If $\tau \ll S$, this gives:

$$v_m \approx v^*(1 - \sqrt{\tau/S}) \quad .$$

The amount of free volume created per second, $\Delta^+ v_f$, can now be calculated from simple rate theory.

Consider the amount of free volume created per second associated with the squeezing open of holes with a volume between v and $v + dv$.

$$d(\Delta^+ v_f) = (\text{number of potential sites}) \times (\text{net number of forward jumps on each of those sites per second}) \times (\text{amount of free volume created per jump})$$

The number of potential sites is equal to the total number of atoms (N) multiplied by the probability that they have a neighboring hole with volume between v and $v + dv$. This factor is obtained from the free volume theory (see Equation (2)).

So

$$\text{number of potential sites} = N\frac{\gamma}{v_f}\exp\left(-\frac{\gamma v}{v_f}\right)dv \qquad (9)$$

The net number of forward jumps is calculated as the difference between a forward and a backward flux, analogously to Equation (4), but with a different $\Delta G = \tau\Omega - \Delta G^e$. So:

net number of forward jumps per potential site per second

$$= \upsilon\left[\exp\left(-\frac{\Delta G^m - \tau\Omega/2 + \Delta G^e/2}{kT}\right) - \exp\left(-\frac{\Delta G^m + \tau\Omega/2 - \Delta G^e/2}{kT}\right)\right] \tag{10}$$

The amount of free volume created per jump is simply the difference between the volume of the atom and the volume of the hole:[28]

$$v^* - v \quad . \tag{11}$$

The total amount of free volume created per second is obtained by integrating all the elementary contributions $d(\Delta^+ v_f)$ over all the hole sizes v, from v_m (the minimum that can be squeezed open) to v^* (above which no free volume is created). This, combined with Equations (9), (10), and (11) gives:

$$\Delta^+ v_f = \int_{v_m}^{v^*} d(\Delta^+ v_f)$$

$$= \int_{v_m}^{v^*} N \frac{\gamma}{v_f} \exp\left(-\frac{\gamma v}{v_f}\right) \upsilon \left[\exp\left(-\frac{\Delta G^m - \tau\Omega/2 + S(v^*-v)^2/2v}{kT}\right)\right.$$

$$\left. - \exp\left(-\frac{\Delta G^m + \tau\Omega/2 - S(v^*-v)^2/2v}{kT}\right)\right](v^*-v)\, dv$$

To simplify the integration, the following assumption is made:

$$\tau \ll S \quad \text{and} \quad v \approx v^* \quad .$$

Therefore,

$$\frac{\gamma}{v_f} \exp\left(-\frac{\gamma v}{v_f}\right) \approx \frac{\gamma}{v_f} \exp\left(-\frac{\gamma v^*}{v_f}\right)$$

$$S\frac{(v^* - v)^2}{2v} \approx S\frac{(v^* - v)^2}{2v^*}$$

This gives:

$$\Delta^+ v_f = N\upsilon \exp\left(-\frac{\Delta G^m}{kT}\right) \frac{\gamma}{v_f} \exp\left(-\frac{\gamma v^*}{v_f}\right) \left\{ \exp\left(\frac{\tau\Omega}{2kT}\right) \frac{v^* kT}{S} \left[1 - \exp\left(-\frac{S(v^* - v_m)^2}{2kTv^*}\right)\right] + \exp\left(-\frac{\tau\Omega}{2kT}\right) \frac{v^* kT}{S} \left[1 - \exp\left(\frac{S(v^* - v_m)^2}{2kTv^*}\right)\right] \right\}$$

In view of Equation (7), which defines v_m, this reduces to the final result:

$$\Delta^+ v_f = \frac{\gamma v^*}{v_f} \frac{2kT}{S} \left[\cosh\left(\frac{\tau\Omega}{2kT}\right) - 1\right] N\upsilon \exp\left(-\frac{\Delta G^m}{kT}\right) \exp\left(-\frac{\gamma v^*}{v_f}\right) \qquad (12)$$

b. Annihilation of Free Volume

The structural rearrangemetns, required for annihilation of extra free volume, consist of a series of diffusive jumps. Let n_D be the number of diffusive jumps necessary to annihilate a free volume equal to v^*. It is expected that n_D should be a small number, between 1 and 10,

This expectation is made plausible by the observation of a two-dimensional amorphous dynamic hard-sphere model.[29] In two dimensions, an amorphous state of high density can only be obtained by using

different size spheres. In contrast with a crystalline system, where a vacancy is a stable entity after many diffusive jumps, in an amorphous system an artificially created "vacancy" is annihilated after a small number of diffusive jumps.

Another useful analogy that can be made comes from Nabarro-Herring creep in crystals. (This analogy must obviously be used with caution, since amorphous systems are topologically quite different from an assembly of microcrystals.) In N.-H. creep, vacancies travel a distance on the order of the grain diameter, and are annihilated at the grain boundaries. In an amorphous system something similar can be imagined, but with a very small equivalent grain size. In crystalline systems, vacancies can annihilate at the grain boundaries because there the structural requirement of crystalline translational symmetry is relaxed. In an amorphous system, this requirement does not exist at all, and hence it is expected that "vacancies" or "extra free volume" can be annihilated in just a few diffusional jumps.

The amount of free volume annihilated per second is

$$\Delta^{-} v_f = \text{(free volume annihilated per jump)} \times \text{(number of jumps per second)}$$

The amount of free volume annihilated per jump is, given the above definitions, v^*/n_D. The number of jumps is $N\Gamma$, where the jump frequency Γ is given by Equation (7). Therefore,

$$\Delta^{-} v_f = \frac{v^*}{n_D} N\upsilon \exp\left(-\frac{\gamma v^*}{v_f}\right) \exp\left(-\frac{\Delta G^m}{kT}\right) \qquad (13)$$

c. Steady State

In steady state, the amount of free volume created is equal to the amount of free volume annihilated:

$$\Delta^{+} v_f = \Delta^{-} v_f$$

Or, from Equations (12) and (13):

$$\frac{\gamma v^*}{v_f} \frac{2kT}{S} \left[\cosh\left(\frac{\tau\Omega}{2kT}\right) - 1 \right] = \frac{v^*}{n_D} \qquad (14)$$

Before the sample is loaded, the average free volume v_f is set by the structure of the quenched metallic glass. At low stresses, the left hand term in (14) is smaller than v^*/n_D, i.e., the extra free volume created by the stress can easily be annihilated by the diffusion, and the average free volume stays at the initial value v_f. As soon as τ exceeds the value for which (14) is obeyed, however, more free volume is being created than can be annihilated by diffusion; hence v_f will keep on increasing until condition (14) is obeyed again. Or, in other words: the free volume v_f is set by the stress τ.

Formally, this can be seen by rewriting Equation (14):

$$\frac{\gamma v^*}{v_f} = \frac{v^*}{n_D} \frac{S}{2kT} \left[\cosh\left(\frac{\tau\Omega}{2kT}\right) - 1 \right]^{-1} \qquad (15)$$

When this explicit expression for $\gamma v^*/v_f$ is substituted in the term $\exp(-\gamma v^*/v_f)$ of the general flow Equation (5), a flow equation for inhomogeneous flow is obtained.

5. DISCUSSION

The only unknown parameter in the flow equations which prevents us from constructing a complete calculated deformation map is ΔG^m. However, if it is assumed that ΔG^m, which may be a function of T and τ, is the same for both homogeneous and inhomogeneous flow, it becomes possible to calculate the boundary between the regions in which each of the mechanisms dominates. The boundary between the two mechanism regions on the deformation map is a line $\tau(T)$, where

$$\dot{\gamma}_{\text{homogeneous}}(\tau, T) = \dot{\gamma}_{\text{inhomogeneous}}(\tau, T) \qquad (16)$$

The only factors in the general flow Equation (5) that are different from one mechanism to the other are Δf and $\exp(-\gamma v^*/v_f)$. So condition (16) becomes then

$$\Delta f_h \exp\left(-\frac{\gamma v^*}{v_f}\right)_h = \Delta f_i \exp\left(-\frac{\gamma v^*}{v_f}\right)_i$$

or

$$\left(\frac{\gamma v^*}{v_f}\right)_i = \left(\frac{\gamma v^*}{v_f}\right)_h - \ell n\left(\frac{\Delta f_h}{\Delta f_i}\right) \qquad (17)$$

Since the free volume v_f is a structural parameter, and since all the data in the vicinity of the mechanism boundary are obtained at temperatures far enough below T_g where the configuration can be considered frozen, $(\gamma v^*/v_f)_h$ is a constant in the equation of the boundary line. Using Equation (15), which determines $(v^*/v_f)_i$, Equation (17) can be rewritten as:

$$\frac{\tau}{\mu} = \frac{4kT}{\mu\Omega} \operatorname{arcsinh}\left(\alpha \frac{kT}{S\Omega}\right)^{-1/2} \qquad (18)$$

with

$$\alpha = 4\left[\left(\frac{\gamma v^*}{v_f}\right)_h - \ell n \frac{\Delta f_h}{\Delta f_i}\right] \frac{n_D}{v^*/\Omega} \qquad (19)$$

(18) is the equation of the mechanism boundary line on the deformation map. It contains only one adjustable parameter: α. The other quantities are known from experiment.

The temperature dependent shear modulus is:

$$\mu(T) = \mu_0 \left(1 - \frac{1}{\mu_0} \frac{d\mu}{dT} (T - 300)\right) ,$$

where μ_0 is the shear modulus at 300 K. The values used here are for $Pd_{77.5}Cu_6Si_{16.5}$:

$$\mu_0 = 3.29 \times 10^{10} \text{Nm}^{-2} \qquad \text{(from Chen et al.}^{30}\text{)}$$

and

$$\frac{1}{\mu_0} \frac{d\mu}{dT} = 2.6 \times 10^{4} \text{K}^{-1} \qquad \text{(from Chen}^{31}\text{)} .$$

The atomic volume is calculated from the density measurements[32] on $Pd_{85.5}Si_{16.5}$: $\Omega = 1.46 \times 10^{-29} \text{m}^3$. The quantity $S = \frac{2}{3}\mu(1+\upsilon/1-\upsilon)$ is calculated using a Poisson's ration $\upsilon = 0.4$, which is typical for metallic glasses.[30]

Figure 5 is an enlarged portion of the empirical deformation map of Fig. 1, showing the boundary between the regions of homogeneous and inhomogeneous flow. The creep data at the bottom of the diagram (Maddin and Masumoto,[7] open squares) are obviously all in the homogeneous deformation region. The transition between inhomogeneous and homogeneous flow, however, shows up in Masumoto and Maddin's tensile data[5] (open circles). The three data points at the highest temperature (533 - 583 K) are ultimate tensile strengths obtained from

stress-strain curves which show very extensive plastic deformation (several percent) before fracture. Therefore, these points belong in the region of homogeneous flow. The parameter α in Equation (13) can now be adjusted such that the resulting boundary line passes between these points and the rest of the tensile data; for the line shown in Fig. 5, $\alpha = 360$.

It remains to be shown now that this is a physically realistic number. Therefore, the quantities in (19), the defining relation for α, must be investigated.

As discussed in Section 3, for homogeneous flow $\Delta f_h = 1$. For inhomogeneous flow Δf is determined by the thickness of the softened layer in the shear band. Since no direct measurements on this are available, the thickness of this layer can only be estimated, e.g., from the height and size of the little "tributaries" in the fracture surface vein-pattern.[18, 12] A layer thickness of 500 Å seems to be a reasonable estimate. If the sample length is 5 cm. and there are only a few shear bands, $\Delta f_i = 10^{-6}$. This is, of course, only an estimate, but, fortunately, the equation is quite insensitive to the exact value of Δf_i.

Chen and Goldstein[14] have measured

$$\frac{\gamma v^*}{v_f} = \frac{3180}{T - 515}$$

in $Pd_{77.5}Cu_6Si_{16.5}$, for homogeneous flow in the region $T \approx T_g$. As mentioned above, in the region under consideration here v_f is considered constant, due to configurational freezing at some temperature around T_g. For $T = 600$, the viscosity of $Pd_{77.5}Cu_6Si_{16.5}$ is $10^{14}\,Nm^{-2}\,sec$;[4] below this the system will be considered configurationally frozen. The appropriate quantity to be used in Equation (19)

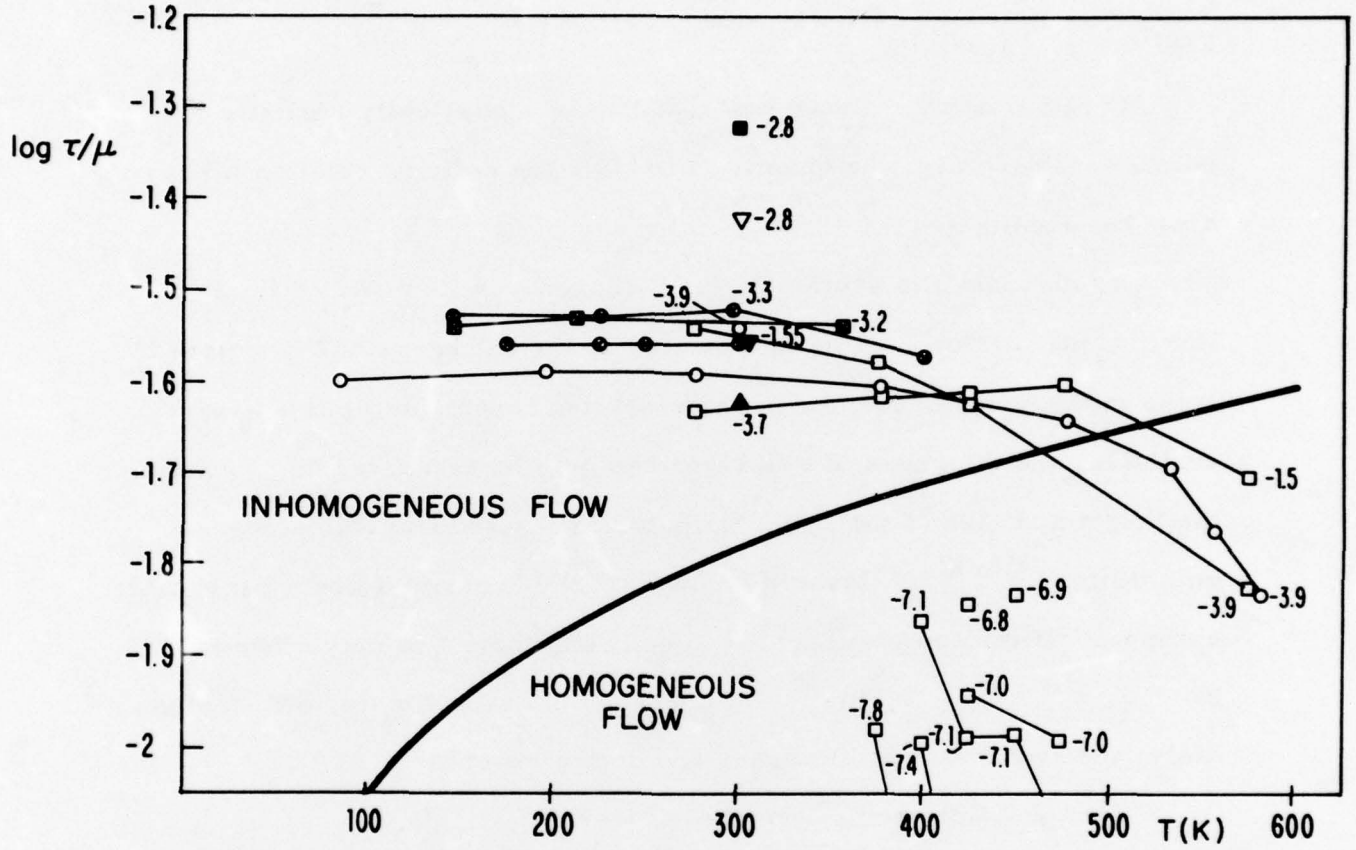

Enlarged portion of the empirical deformation map for Pd-based metallic glasses. The equivalent shear stress (τ) and shear strain ($\dot{\gamma}$) have been calculated from the uniaxial values by the von Mises criterion ($\tau = \sigma/\sqrt{3}$; $\dot{\gamma} = \sqrt{3}\,\dot{\epsilon}$). The strain rate contours connect data points from the same reference. The shear modulus is from Refs. 30 and 31. The heavy line is the boundary between regions of homogeneous and inhomogeneous is calculated from Eq. (18).

Figure 5.

is therefore:

$$\left(\frac{\gamma v^*}{v_f}\right)_h = \frac{3180}{600 - 515} = 37.4$$

Substituting the values for α, Δf_h, Δf_i, and $(\gamma v^*/v_f)_h$ in (19) leaves

$$\frac{v^*/\Omega}{n_D} = 0.26 \quad .$$

This is a physically reasonable result. The equivalent hard-sphere volume of a late transition metal as Pd probably takes up a large fraction of the atomic volume, say, $v^*/\Omega \approx .8$. This leaves $n_D \approx 3$, which is consistent with the physical considerations of Section 4b, where it was argued that the number of diffusional jumps necessary to annihilate a free volume equal to v^* should be somewhere between 1 and 10.

It may be worth noting that the mechanism boundary on the deformation map has a positive slope, i.e., with increasing temperature it is necessary to go to higher stresses to get inhomogeneous flow. Physically, this is not unexpected, since the diffusional relaxation process becomes relatively more important at high temperatures.

At this stage, the stress exponent $n = \partial \log \dot{\gamma}/\partial \log \tau$ for the two flow modes can also be calculated, if it is assumed that ΔG^m is independent of τ. The results of this calculation are shown in Fig. 6. The stress exponent for homogeneous flow is $n \approx 1$, as it should be for Newtonian viscous flow. For inhomogeneous flow $n \approx 50$, which indicates that it approaches ideally plastic behavior.

Finally, it should be emphasized that the present mechanism involves monatomic systems, and does not explicitly include any chemical effects. However, chemical ordering is reflected partially in the

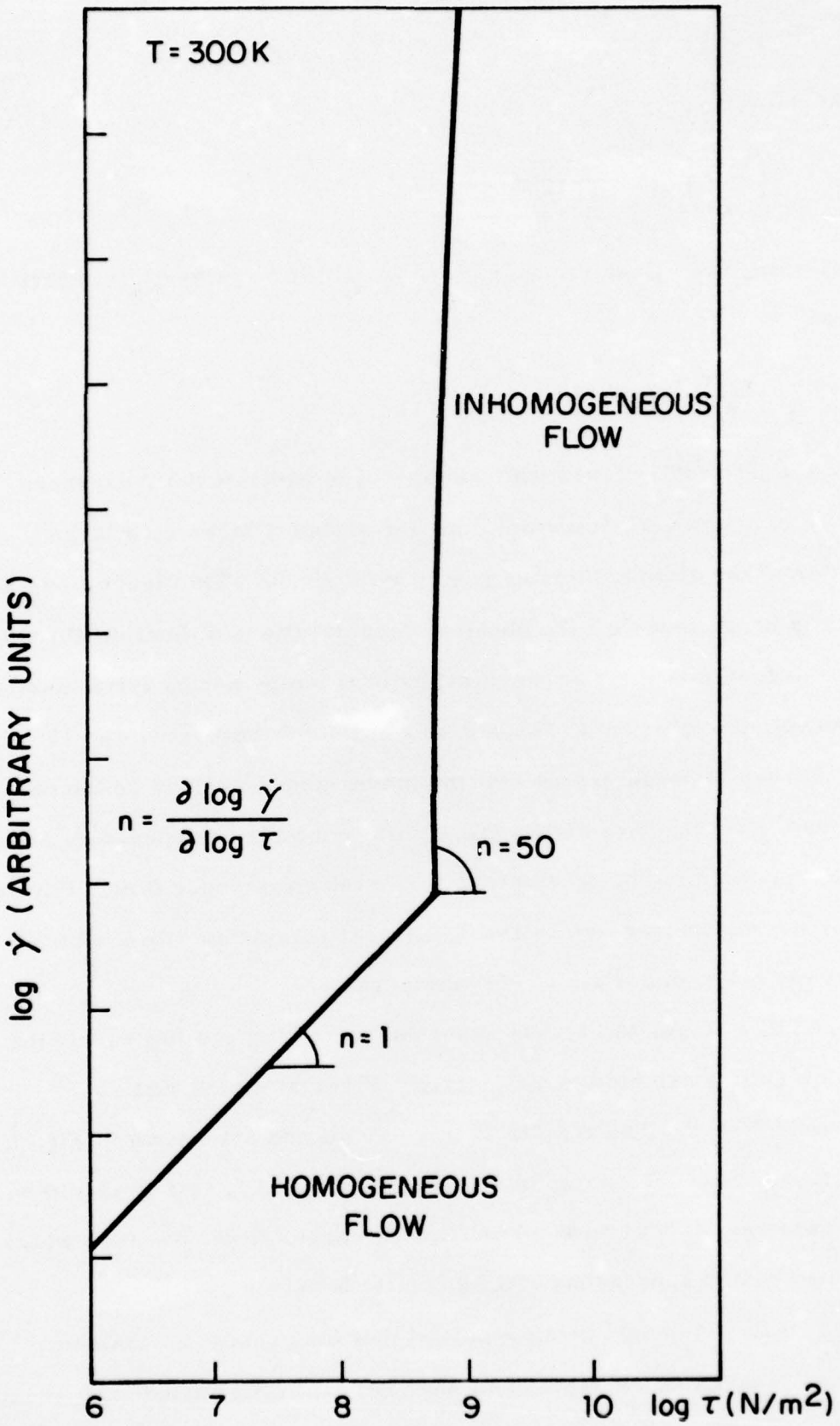

Stress-strain rate dependence of homogeneous and inhomogeneous flow, calculated from the theoretical models.

Figure 6.

free volume formulation, for example, if an efficient packing of atoms of different size (as Pd and Si) requires a non-random chemical environment for the two atoms. In this case, creation of free volume is equivalent to creation of chemical disorder. On the other hand, there are probably some specific chemical effects, as the metal-metalloid bonding, which should be included in ΔG^m. The differences in strength found by changing the metalloid components in a metallic glass are probably of this nature. However, it is also possible that an increased diffusivity of one type of metalloid to the other might lead to an increased diffusional relaxation, and hence a higher strength. For example, the exceptionally high strength of Fe_4B glass[33] might conceivably be caused by the higher diffusivity of the small B-atom.

Acknowledgements

It is a pleasure to acknowledge several useful suggestions and criticisms from Professors D. Turnbull and M. F. Ashby. I am indebted to Dr. H. J. Frost for his help in constructing the deformation maps and for several helpful discussions.

This work has been supported in part by grants from the Office of Naval Research under Contract N00014-67-A-0298-0036 and from the National Science Foundation under Contract DMR-72-03020.

I also want to acknowledge a postdoctoral Fellowship from the I. B. M. Corporation.

References

1. M.F. Ashby, Acta Met. 20, 887 (1972).
2. H.J. Frost and M.F. Ashby, Proc. of the John E. Dorn Symposium, J.C.M. Li and A.K. Mukherjee (eds.), A.S.M., Cleveland, Ohio, 70 (1975).
3. M.F. Ashby and H.J. Frost, "Constitutive Equations in Plasticity", A.S. Argon (ed.), M.I.T. Press, Cambridge, Mass., 117 (1975).
4. H.S. Chen and M. Goldstein, J. Appl. Phys. 43, 1642 (1971).
5. T. Masumoto and R. Maddin, Acta Met. 19, 725 (1971).
6. H.J. Leamy, H.S. Chen and T.T. Wang, Met. Trans. 3, 699 (1972).
7. R. Maddin and T. Masumoto, Mat. Sci. Eng. 9, 153 (1972).
8. H.S. Chen, Scripta Met. 7, 931 (1973).
9. C.A. Pampillo and H.S. Chen, Mat. Sci. Eng. 13, 181 (1974).
10. H.S. Chen and D.E. Polk, J. Non-Cryst. Solids 15, 174 (1974).
11. C.A. Pampillo, J. Mat. Sci. 10, 1194 (1975).
12. C.-P.P. Chou and F. Spaepen, Acta Met. 23, 609 (1975).
13. H.S. Chen and D. Turnbull, Acta Met. 17, 1021 (1969).
14. D.E. Polk and D. Turnbull, Acta Met. 20, 493 (1972).
15. H.S. Chen and D. Turnbull, J. Chem. Phys. 48, 2560 (1968).
16. J. Logan and M.F. Ashby, Acta Met. 22, 1047 (1974).
17. C.A. Pampillo and D.E. Polk, Acta Met. 22, 741 (1974).
18. C.A. Pampillo and A.C. Reimschuessel, J. Mat. Sci. 9, 718 (1974).
19. F. Spaepen, Acta Met. 23, 615 (1975).
20. A.S. Argon and M. Salama, "Proc. 2nd Int. Conf. on Rapidly Quenched Metals", N.J. Grant and B.C. Giessen (eds.), Section II, Mat. Sci. Eng. 23, 219 (1976).
21. F. Spaepen and D. Turnbull, Scripta Met. 8, 563 (1974).
22. T. Masumoto and R. Maddin, Mat. Sci. Eng. 19, 1 (1975).

23. C.A. Pampillo, Scripta Met. 6, 915 (1972).

24. S. Takayama and R. Maddin, Acta Met. 23, 943 (1975).

25. M.H. Cohen and D. Turnbull, J. Chem. Phys. 31, 1164 (1959).

26. D. Turnbull and M.H. Cohen, J. Chem. Phys. 34, 120 (1961).

27. D. Turnbull and M.H. Cohen, J. Chem. Phys. 52, 3038 (1970).

28. J.D. Eshelby, Solid State Physics, F. Seitz and D. Turnbull (eds.), 3, 115 (1956).

29. For a description of the original mechanical model, see: D. Turnbull and R.L. Cormia, J. Appl. Phys. 31, 674 (1960).

30. H.S. Chen, J.T. Krause and E. Coleman, J. Non-Cryst. Solids 18, 157 (1975).

31. H.S. Chen, Scripta Met. 9, 411 (1975).

32. H.S. Chen, J.T. Krause and E. Coleman, Scripta Met. 9, 787 (1975).

33. L.A. Davis, R. Ray, C.-P. Chou, and R.C. O'Handley, Scripta Met. 10, 541 (1976).

DISTRIBUTION LIST

Contract N00017-67-A-0298-0036

Defense Documentation Center
Cameron Station
Alexandria, Virginia 22314 (12)

Office of Naval Research
Department of the Navy

Attn: Code 471 (3)
Code 105 (6)
Code 470

Director
Office of Naval Research
Branch Office
495 Summer Street
Boston, Massachusetts 02210

Director
Office of Naval Research
Branch Office
536 South Clark Street
Chicago, Illinois 60605

Office of Naval Research
San Francisco Area Office
760 Market Street, Room 447
San Francisco, California 94102

Naval Research Laboratory
Washington, D.C. 20390

Attn: Code 6000
Code 6100
Code 6300
Code 6400
Code 2627 (6)

Attn: Mr. F.S. Williams
Naval Air Development Center
Code 302
Warminster, Pennsylvania 18974

Naval Air Propulsion Test Center
Trenton, New Jersey 08628
Attn: Library

Naval Weapons Laboratory
Dahlgren, Virginia 22448
Attn: Research Division

Naval Construction Batallion
Civil Engineering Laboratory
Port Hueneme, California 93043
Attn: Materials Division

Naval Electronics Laboratory Center
San Diego, California 92152
Attn: Electronic Materials Sciences Div.

Naval Missile Center
Materials Consultant
Code 3312-1
Point Mugu, California 93041

Commanding Officer
Naval Ordnance Laboratory
White Oak
Silver Spring, Maryland 20910
Attn: Library

Naval Ship R. and D. Center
Materials Department
Annapolis, Maryland 21402

Naval Undersea Center
San Diego, California 92132
Attn: Library

Naval Underwater System Center
Newport, Rhode Island 02840
Attn: Library

Naval Weapons Center
China Lake, California 93555
Attn: Library

Naval Postgraduate School
Monterey, California 93940
Attn: Materials Sciences Dept.

Naval Air Systems Command
Washington, D.C. 20360

Attn: Code 52031
Code 52032
Code 320

Naval Sea System Command
Washington, D.C. 20362
Attn: Code 035

Naval Facilities
Engineering Command
Alexandria, Virginia 22331
Attn: Code 03

Scientific Advisor
Commandant of the Marine Corps
Washington, D.C. 20380
Attn: Code AX

Naval Ship Engineering Center
Department of the Navy
Washington, D.C. 20360
Attn: Director, Materials Sciences

Army Research Office
Box CM, Duke Station
Durham, North Carolina 27706
Attn: Metallurgy and Ceramics Div.

Army Materials and Mechanics
Research Center
Watertown, Massachusetts 02172
Attn: Res. Programs Office (AMXMR-P)

Commanding General
Department of the Army
Frankford Arsenal
Philadelphia, Pennsylvania 19137
Attn: ORDBA-1320

Office of Scientific Research
Department of the Air Force
Washington, D.C. 20333
Attn: Solid State Div. (SRPS)

Aerospace Research Labs
Wright-Patterson AFB
Building 450
Dayton, Ohio 45433

Air Force Materials Lab (LA)
Wright-Patterson AFB
Dayton, Ohio 45433

NASA Headquarters
Washington, D.C. 20546
Attn: Code RRM

NASA
Lewis Research Center
21000 Brookpark Road
Cleveland, Ohio 44135
Attn: Library

National Bureau of Standards
Washington, D.C. 20234

Attn: Metallurgy Division
Inorganic Materials Division

Atomic Energy Commission
Washington, D.C. 20545
Attn: Metals and Materials Branch

Defense Metals and Ceramics
Information Center
Battelle Memorial Institute
505 King Avenue
Columbus, Ohio 43201

Director
Ordnance Research Laboratory
P.O. Box 30
State College, Pennsylvania 16801

Director Applied Physics Lab.
University of Washington
1013 Northeast Fortieth Street
Seattle, Washington 98105

Metals and Ceramics Division
Oak Ridge National Laboratory
P.O. Box X
Oak Ridge, Tennessee 37830

Los Alamos Scientific Lab.
P.O. Box 1663
Los Alamos, New Mexico 87544
Attn: Report Librarian

Argonne National Laboratory
Metallurgy Division
P.O. Box 229
Lemont, Illinois 60439

Brookhaven National Laboratory
Technical Information Division
Upton, Long Island
New York 11973
Attn: Research Library

Library
Building 50, Room 134
Lawrence Radiation Laboratory
Berkeley, California

Professor G.S. Ansell
Rensselaer Polytechnic Institute
Dept. of Metallurgical Engineering
Troy, New York 12181

Professor H.K. Birnbaum
University of Illinois
Department of Metallurty
Urbana, Illinois 61801

Dr. E.M. Breinan
United Aircraft Corporation
United Aircraft Research Lab.
East Hartford, Connecticut 06108

Professor H.D. Brody
University of Pittsburgh
School of Engineering
Pittsburgh, Pennsylvania 15213

Professor J.B. Cohen
Northwestern University
Dept. of Material Sciences
Evanston, Illinois 60201

Professor M. Cohen
Massachusetts Institute of Technology
Department of Metallurgy
Cambridge, Massachusetts 02139

Professor B.C. Giessen
Northeastern University
Department of Chemistry
Boston, Massachusetts 02115

Dr. G.T. Hahn
Battelle Memorial Institute
Department of Metallurgy
515 King Avenue
Columbus, Ohio 43201

Professor R.W. Heckel
Carnegie-Mellon University
Schenley Part
Pittsburgh, Pennsylvania 15213

Dr. David G. Howden
Battelle Memorial Institute
Columbus Laboratories
505 King Avenue
Columbus, Ohio 43201

Professor C.E. Jackson
Ohio State University
Dept. of Welding Engineering
190 West 19th Avenue
Columbus, Ohio 43210

Professor G. Judd
Rensselaer Polytechnic Institute
Dept. of Materials Engineering
Troy, New York 12181

Dr. C.S. Kortovich
TRW, Inc.
23555 Euclid Avenue
Cleveland, Ohio 44117

Professor D.A. Koss
Michigan Technological University
College of Engineering
Houghton, Michigan 49931

Professor A. Lawley
Drexel University
Dept. of Metallurgical Engineering
Philadelphia, Pennsylvania 19104

Dr. H. Margolin
Polytechnic Institute of New York
333 Jay Street
Brooklyn, New York 11201

Professor K. Masabuchi
Massachusetts Institute of Technology
Department of Ocean Engineering
Cambridge, Massachusetts 02139

Dr. G.H. Meier
University of Pittsburgh
Dept. of Metallurgical and Materials Engineering
Pittsburgh, Pennsylvania 15213

Professor J.W. Morris, Jr.
University of California
College of Engineering
Berkeley, California 94720

Professor K. Ono
University of California
Materials Department
Los Angeles, California 90024

Professor W.F. Savage
Rensselaer Polytechnic Institute
School of Engineering
Troy, New York 12181

Dr. C. Shaw
Rockwell International Corp.
P.O. Box 1085
1049 Camino Dos Rios
Thousand Oaks, California 91360

Professor O.D. Sherby
Stanford University
Materials Sciences Dept.
Stanford, California 94300

Professor J. Shyne
Stanford University
Materials Sciences Department
Stanford, California 94300

Dr. W.A. Spitzig
U.S. Steel Corporation
Research Laboratory
Monroeville, Pennsylvania 15146

Dr. E.A. Starke, Jr.
Georgia Institute of Technology
School of Chemical Engineering
Atlanta, Georgia 30332

Professor N.S. Stoloff
Rensselaer Polytechnic Institute
School of Engineering
Troy, New York 12181

Dr. E.R. Thompson
United Aircraft Research Lab.
400 Main Street
East Hartford, Connecticut 06108

Professor David Turnbull
Harvard University
Division of Engineering and Applied Physics
Cambridge, Massachusetts 02139

Dr. F.W. Wang
Naval Ordnance Laboratory
Physics Laboratory
White Oak
Silver Spring, Maryland 20910

Dr. J.C. Williams
Rockwell International
Science Center
P.O. Box 1085
Thousand Oaks, California 91360

Professor H.G.F. Wilsdorf
University of Virginia
Department of Materials Science
Charlottesville, Virginia 22903

Dr. M.A. Wright
University of Tennessee
Space Institute
Dept. of Metallurgical Engineering
Tullahoma, Tennessee 37388